Effectiveness of Two Forms of Grouted Reinforced Confinement Methods to Hollow Concrete Masonry Panels

Thangarajah Janaraj[1] and Manicka Dhanasekar[*2]

Abstract

This paper presents a study on the effectiveness of two forms of reinforced grout confining systems to the hollow concrete block masonry. The systems considered are: (1) a layer of grout directly confining the unreinforced masonry and (2) a layer of grout indirectly confining the unreinforced masonry through block shells. The study involves experimental testing and finite element (FE) modelling of six diagonally loaded masonry panels containing the two confining systems. The failure mode, the ultimate load and the load-deformation behaviors of the diagonally loaded panels were successfully simulated using the finite element model. In-plane shear strength and stiffness of the masonry thus determined are used to evaluate some selected models of the confined masonry shear including the strut and tie model reported in the literature. The evaluated strut width is compared with the prediction of the FE model and then extended for rational prediction of the strength of confined masonry shear walls.

Keywords: Confined masonry; grout confinement; grouted shell confinement; diagonal testing; in-plane shear; diagonal strut.

[1] Research Associate, *School of Civil engineering and Built Environment, Queensland University of Technology, Australia. E-mail:* thangarajah. janaraj@ qut.edu.au

[2] Corresponding Author: Professor, *School of Civil engineering and Built Environment, Queensland University of Technology, Gardens Point campus, 2, George St., Brisbane, QLD 4000, Australia. Ph. +61 7 3138 6666, E-mail:* m.dhanasekar@qut.edu.au

Introduction

Vulnerability of unreinforced masonry (URM) buildings to horizontal loading is mainly attributed to the low tensile and shear strengths of the unreinforced masonry. To improve the tensile and shear strengths, a grid of horizontal and vertical reinforcements is embedded into the URM wall panels. Two methods of embedment are used. In the first method, the URM is built first and some selected hollow cores are then filled with reinforced grout (Dhanasekar and Haider 2008a; Nolph and ElGawady 2012; Shing et al. 1990).This type of construction is known as wide spaced reinforced masonry or partially grouted masonry and adopted in moderate seismic countries. In the second method the URM is constructed first with discrete gaps as a priori, which are then filled with reinforced concrete; such walls are generally known as 'confined masonry' in the literature, with claims that they outperform other types of masonry constructions in seismic zones (Moroni et al. 2004; Tena-Colunga et al. 2009). The confined masonry practiced in severe seismic countries accommodates confining elements that include several longitudinal bars and shear ties whereas the partially grouted masonry generally contains just a single reinforcing bar with no shear ties. This paper presents a study carried out to compare the effectiveness of these two systems of construction. In this paper, the active confining system is termed as the 'grout confined masonry (GCM)' and the passive confining system is termed as the 'grouted shell confined masonry (GSCM)'.

It is reported in the literature that the load resisting capacity of the confined masonry is maintained until the masonry panels experience severe cracking (Medeiros et al. 2013; Yoshimura et al. 1996). Irrespective of the percentage of reinforcement, no evidence of yielding of the steel in the confining element can be found in the literature; this shows that the confining elements used to date remain with very limited cracking until the collapse of the masonry, although the masonry strength is enhanced by the confining elements. Since

there is clear evidence in the literature that the steel in the confining elements do not participate significantly, in this investigation only a single bar with no shear ties has been used.

The effectiveness of two confining systems (GCM and GSCM) to the URM has been examined through diagonal compression tests and finite element modelling. Further the predictions of the existing confined masonry models are compared with the experimental test results and suggestions are made on its prediction capability for these two types of masonry systems.

Experiments

A brief overview of the experiments is given here as the experimental details are reported elsewhere (Janaraj 2014; Janaraj and Dhanasekar 2014). All test specimens were constructed in half scale to accommodate sufficient number of mortar joints in a reasonable size masonry panel. Half scale blocks of dimension $185 \times 90 \times 90.5$ mm (Length $\times$ Height $\times$ Width). The unconfined compressive strength of the blocks were determined in accordance with AS/NZS (2003a) and the mean compressive strength was found as 18.7 MPa from six specimens with a COV of 7.4%. Mean modulus of rupture was determined as 2.8 MPa with a COV of 10.9%.from eight specimens of three blocks long each , tested in accordance with AS/NZS (2003b).

All masonry specimens were constructed using 5mm thick 1:1:6 (cement:lime:sand) mortar joints by an average skilled mason. Scaled down fine aggregates and 10 mm maximum size coarse aggregates were used in the grout of high slump of 260mm as specified in ASTM (2006). The same mix was used for both the GCM and the GSCM systems. The mean compressive strength of the mix was determined as 30.1 MPa (COV 6%) from 12 cylinder specimens in accordance with AS (2009).

Two tensile coupon tests from 12 mm diameter reinforcement bar (N12) were carried out in accordance with ASTM (2009); its mean yield strength (f_{ys}) was determined as 500 MPa (COV 0.6 %) and the mean modulus of elasticity (E_s) was 200 GPa (COV 1.4%).

Characterization of un-grouted and grouted masonry

All masonry specimens were tested at 14 days of age in accordance with the AS (2011). The specimens were cured under plastic wrapping to prevent moisture evaporation for the first 7days followed by 7 days of air curing. Compressive strength of the hollow masonry (f_{hm}) and the grouted masonry (f_{gm}) was determined using 4 high stack bonded prisms. The mean strength f_{hm} was 9.2 MPa (determined from 12 specimens with a COV of 16 %) and the mean value of f_{gm} was 8.8 MPa (determined from 6 specimens with a COV of 17.2 %). The compressive strength of the grouted masonry was lower than that of the hollow masonry due to: (1) differential lateral displacements of the grout and the shell and, (2) the truncated tapered pyramid shaped grout exercising lateral component of force on the shell under vertical movement (known as 'wedging action'); these two actions lead to shell spalling and lower strength. The mean hollow masonry elastic modulus (E_{hm}) and the mean grouted masonry elastic modulus (E_{gm}) were 3277 MPa and 14590 MPa, respectively. Four point bending tests were conducted on six specimens of each containing 7 stack bonded blocks. The mean flexural tensile strength (f_{mt}) of the masonry was determined as 0.5MPa with a COV of 22 %.

Design and construction of diagonal compression test specimens

The diagonal compression tests are widely used to study the tensile/ shear properties of the conventional unreinforced masonry (ASTM 2002; Corradi et al. 2008; Tena-Colunga et al.

2009). These diagonal compression tests are also used to examine the effectives of the masonry panels containing various strengthening elements (Dizhur et al. 2013). In this research, diagonal compression tests were conducted to examine the effectiveness of the two confining elements (GCM and GSCM) to the unreinforced masonry.

Six panels of a pair of three configurations, shown in **Fig. 1**, were tested. The dimensions of the unconfined masonry (UCM) panels were kept constant as 660 mm square in all panels as shown in **Fig. 1**-A. Each UCM panel was 3.5 blocks wide and seven layers high. The GSCM panel shown in **Fig. 1**-B also contained an unreinforced panel of 660 mm × 660 mm; with confined elements, the gross dimensions of the specimen was 850 mm × 850 mm where the edge hollow cores were filled with grout embedding a 12 mm diameter reinforcement bar positioned at their center. The GCM panel shown in **Fig. 1**-C had a gross dimension of 850mm quare which included grout confining elements of 95 mm width surrounding the 660 mm square unreinforced panel. Since each configuration contained two panels, the first one was named as 'A' and the second as 'B'. The methods of constructing the GSCM and GCM confined masonry panels are shown in in **Fig. 2**-A and **Fig. 2**-B, respectively.

Test set-up and instrumentation

The scheme of instrumentation is shown in **Fig. 3**. Three linear variable differential transducers (LVDTs) were used to measure the state of strain at the center of the panel; the displacements read by the LVDTs were converted to normal, parallel and shear strains with reference to the direction of bed joints of the masonry using their respective gage lengths. Two LVDTs measured the displacement of the loading shoe and one LVDT monitored any potential out-of-plane movement of the panel. String-Pots (SP) were used to measure shortening and elongation of the loaded and unloaded diagonals of the panels.

At selected location, the reinforcing bars were provided with strain gages (SGs). The attached SGs were protected from ingress of water using neutral waterproofing sealants. For each step of load, sixteen strain gages were read on each confined masonry specimens; two sets of four of them measured steel strains near the loading and support shoes respectively and the rest of the two sets of four of them measured steel strains at the unloaded corners of the specimen.

Experimental Results and Discussion

To study the effectiveness of confinement, the diagonal peak load of each panel is considered as shown in **Table 1** The UCM panels achieved an average peak load of 48.6 KN; the GSCM panels achieved an average peak load of 60.8 kN; and the GCM panels achieved an average peak load of 78.1 kN. The average diagonal load capacity of the GSCM and the GCM panels were 25 % and 61% higher than that of the UCM panels. It can be said that the GSCM system is less effective due to passive confinement compared to the GCM which offered active confinement. Since the only limited number of specimens has been used in the experiments, results may be confirmed through an extensive experimental program.

The ductility is defined as the ratio of ultimate displacement to yield displacement. The ultimate load was considered as 80% of the peak load. The stiffness degradation (S_i is stiffness degradation parameter at i^{th} loading stage of the panel) was examined using Eq. (1),

$$S_i = \left(\frac{K_i - K_y}{K_y} \right) \times 100 \qquad \text{Eq. (1)}$$

Where K_i stands for stiffness at i^{th} loading step and K_y stands for stiffness at the yielding of the panel. The average stiffness of UCM and GSCM panels at yielding $\left(K_y\right)$ was 16 $kNmm^{-1}$, and the GCM panels' average stiffness at yielding was 27 $kNmm^{-1}$ which is

69% higher. The average stiffness at the peak load (K_p) of the UCM, the GSCM and the GCM panels were 14.9 $kNmm^{-1}$, 14.1 $kNmm^{-1}$ and 22.9 $kNmm^{-1}$, respectively. Individual panel data are reported in **Table 1**.

Using Eq-1, the stiffness degradation at the peak load (S_p) and at the ultimate load (S_u) of these panels were determined. The average S_p of the UCM, the GSCM and the GCM panels was -6.9%, -12.2% and -15%, respectively; the GCM active confinement has exhibited the lowest degradation. Further studies were conducted at the ultimate load capacity of the panels.

The failure of the unreinforced masonry of the GSCM and the GCM panels were examined using the state of strain obtained from the three LVDT measurements at the center of the panel. The diagonal load versus the principal strain diagrams of the GSCM and the GCM panels are shown in **Fig. 4**. **Fig. 4**-A, shows the maximum principal strain and **Fig. 4**-B shows the minimum principal strains at the center of the panels. The points of change from elastic strain to inelastic strains correspond to approximately 100μ and its corresponding diagonal load of the GSCM and the GCM panels were 36 kN and 61 kN, respectively. The diagonal yield load capacity of the GSCM and the GCM panels were 58.7 kN and 69.2 kN, respectively.

The unreinforced masonry located in the GSCM panels experienced larger tensile strain at 61 % of its yield capacity whereas those in the GCM panels experienced larger tensile strains at 88 % of its yield capacity. It can be seen from and **Fig. 4**-B, the actively confined GCM panel has exhibited a higher level of post-yield strain hardening, which is not obvious for the partially grouted GSCM panel. It shows that GCM active confinement is more effective than the GSCM passive confinement.

166 At the ultimate load, the GSCM panel experienced a maximum principal strain of
167 8300μ whereas the GCM panel exhibited a strain of 7560μ which is nearly same as that of
168 the GSCM panel's failure strain.

169 The reinforcement strain is also examined as it explicitly shows the behavior of the
170 confining element. The strain gage located in the SG2 position was considered for GSCM
171 and GCM panels and the average response is shown in **Fig. 5**. The reinforcement exhibited
172 positive (tensile) strains at a diagonal load of 36 kN and 60 kN for GSCM and GCM,
173 respectively. These observations are consistent with larger tensile principal strains (100 μ)
174 observed in the unreinforced masonry in the panel. This phenomenon can be explained as the
175 masonry initially resists the load by itself while the confinement elements do not play a
176 significant role. However, once the inelastic behavior in the unreinforced masonry was
177 observed (cracking), the unreinforced masonry section pushes the confining elements
178 sideways. At this stage, confining element becomes engaged in resisting forces.

179 The GSCM panel remained in the elastic region even after the confining element
180 became active. Further 39 % of load was resisted by the GSCM panel to reaches its yield
181 capacity of 58.7 kN. However, the GCM panel resisted an additional 12% load to reach its
182 yield capacity of 69.2 kN. There was no yielding of reinforcement observed from the strain
183 gage data in both panels.

184

185 ## Modeling Approach

186 A macro modeling method considering the masonry as an anisotropic continuum was used in
187 the FE simulations. This FE model was based on an explicit formulation presented by
188 Dhanasekar and Haider (2008b). The masonry, the GSCM confining element, the GCM
189 confining element and the steel reinforcement were modeled as distinctly different materials.
190 Initially a mesh convergence study was conducted and the optimum mesh size for the

masonry (95 mm high × 110 mm long) and grouted core (95 mm high × 95 mm long) were selected. The confined masonry panels (GSCM and GCM) contained similar mesh. Plane stress reduced integration elements available in ABAQUS were used.

Hollow masonry and GSCM confining element were modelled using the multi-surface plasticity model proposed by Lourenço (1996). This plasticity model contained Hill type failure surface for compression and Rankine failure surface for tension. These equations are incorporated in a VUMAT subroutine suitable for ABAQUS/Explicit. The Hill type yield surface is written as in Eq. (2),

$$f = A\sigma_p^2 + B\sigma_p\sigma_n + C\sigma_n^2 + D\tau_{np}^2 - 1 = 0 \quad \text{Eq. (2)}$$

in which $A = 1/(f_{cp}(\kappa_c))^2$, $B = \beta/(f_{cp}(\kappa_c) f_{cn}(\kappa_c))$, $C = 1/(f_{cn}(\kappa_c))^2$ and $D = \gamma/(f_{cp}(\kappa_c) f_{cn}(\kappa_c))$ are material parameters. Compressive strength normal to bed joint (f_{cn}) was determined from the prisms tests and the compressive strength parallel to bed joint (f_{cp}) was calculated using an f_{cp}/f_{cn} ratio of 0.80. The f_{cn} for the hollow masonry and the grouted confining element was 9.2 MPa and 8.7 MPa, respectively.

Scalar κ_c controls the hardening and softening; the parameters and γ control the coupling between normal stress and shear stress contribution to failure. β can be determined from the biaxial compression test; in the absence of such a test a value of -1.17 was considered (Lourenço 1996). γ was calculated from $f_{cn} f_{cp}/\tau_u^2$ where τ_u is material pure shear strength. $\gamma = 4$ was considered for hollow masonry and $\gamma = 2$ was considered for grouted confining element. The Rankine failure criteria can be written as in Eq. (3),

$$f = \frac{\sigma_a + \sigma_b}{2} + \sqrt{\left(\frac{\sigma_a - \sigma_b}{2}\right)^2 + \alpha\tau_{np}} \quad \text{Eq. (3)}$$

in which $\sigma_a = \sigma_p - \bar{\sigma}_{t1}(\kappa_t)$, $\sigma_b = \sigma_n - \bar{\sigma}_{t2}(\kappa_t)$ and $\alpha = \frac{f_{tp} \times f_{tn}}{\tau_u^2}$; where τ_u is material pure shear strength. σ_n and σ_p indicate the stress normal to bed joint and parallel to bed joint, respectively. For the concrete masonry, $\alpha = 1.25$ was considered as recommended in Lourenço (1996). For the grouted masonry confining elements in the GSCM panels, a similar value of α was considered. $\bar{\sigma}_{t1}$ and $\bar{\sigma}_{t2}$ were calculated using $f_{tp} \exp\left(-\frac{\bar{h} \times f_{tp}}{G_{tp}} \kappa_t\right)$ and $f_{tn} \exp\left(-\frac{\bar{h} \times f_{tn}}{G_{tn}} \kappa_t\right)$, respectively. Tensile strength normal to bed joint (f_{tn}) and fracture energy normal to bed joint (G_{tn}) were determined from the experimental test results. For this purpose, the values obtained from four point bending test was divided by 1.5 to take direct tensile stress as suggested in Van der Pluijm (1997). For the masonry the converted four point bending test permits the variation of f_{tn} from 0.21 MPa to 0.41 MPa. The calibrated optimum value of f_{tn} was 0.27 MPa and the G_{tn} was 0.30 Nmm/mm^2. The tensile strength parallel to bed joint (f_{tp}) and fracture energy parallel to bed joint (G_{tp}) were determined from the f_{tp} / f_{tn} and G_{tp} / G_{tn} ratios suggested in Lourenço (1996). For the hollow masonry f_{tp} and G_{tp} were found as 0.5 MPa and 0.65 Nmm/mm^2, respectively; for grouted masonry f_{tn}, f_{tp}, G_{tn} and G_{tp} were found as 0.32 MPa, 0.55 MPa, 0.55 Nmm/mm^2 and 1.00 Nmm/mm^2, respectively.

The characteristic length for linear elements $(\bar{h})$ was determined from $\sqrt{Area\ of\ the\ element}$. Based on the selected mesh sizes representing the masonry and the grouted confining elements, it was found as 102 mm for masonry and 95 mm for grouted confinement. The elastic modulus normal (E_n) to bed joint was considered from the prism

232 tests of the hollow masonry and the grouted masonry. The elastic modulus parallel to bed
233 joint $\left(E_p\right)$ was calculated from E_p / E_n ratio published in (Haider 2007)and (Lourenço 1996).
234 Poisson's ratio of the hollow masonry and the grouted masonry were considered as 0.20 and
235 0.22 respectively.

236 Concrete was modeled using the damage plasticity model available in the ABAQUS.
237 From concrete cylinder tests, the mean elastic modulus $\left(E_c\right)$ and the mean compressive
238 strength of the concrete was found as 26000 MPa and 30.1 MPa, respectively. Reinforcement
239 bars were modeled using truss elements (T2D2 in ABAQUS) capable of resisting tension but
240 would buckle in compression. It was not possible to detail ties to the longitudinal steel;
241 therefore, the reinforcement was incapable of withstanding compressive stress; the
242 compression stress in the steel reinforcing bars was therefore, limited to a maximum of 1
243 *MPa*. From the tensile coupon test conducted on the reinforcement, the yield strength,
244 ultimate strength and the failure strength were found as 500 MPa, 550 MPa and 400 MPa,
245 and its corresponding strains were 0.0025, 0.01 and 0.012, respectively. The elastic modulus
246 was determined as 200 GPa. These parameters were used to model the reinforcement. Further
247 details of the all selected parameters can be found elsewhere (Janaraj 2014; Janaraj and
248 Dhanasekar 2014).

249 The FE model outputs are validated using the experimental results presented in the
250 previous section and is reported in the sub sections below.

251

252 ## Model Validation

253 **Load-displacement**

254 **Fig. 6**-A shows the diagonal (vertical) load - displacement responses along the UCM panels
255 and its FE model prediction; good agreement is obtained. Both the FE model and the
256 experiment results show that these panels reached its average peak diagonal load of 47 kN at

a diagonal displacement of approximately 3.5 mm (FE-3.5mm, UCM-A- 3.2 mm & UCM-B-3.6mm).

The load displacement curves of the two GSCM and GCM panels are reported together the corresponding FEM predictions in **Fig. 6**-B and **Fig. 6**-C, respectively. For the GSCM panels the FEM predicted the peak load of 59.6 kN whilst the experimental average capacity was 60.7 kN. The peak load in the FEM was achieved at a diagonal displacement of 4.6 mm whereas the experimental peak was achieved at 4.4 mm. Both the FEM and the experiment predicted ultimate failure at a diagonal displacement of 5.3 mm. For the GCM panels, the FEM predicted the peak load of 72.1 kN whilst the experimental average peak load was 78.1 kN, which is a deviation of 8 %, which is considered quite normal in concrete masonry research and acceptable as the prediction is conservative. The peak load of FEM was achieved at a diagonal displacement of 3.7 mm whereas the experimental displacement corresponding to peak load (average of A and B) was 3.5 mm. The FE model was predicting the load capacity and the failure displacement of the panels very well. Testing of additional panels is desired to further confirm the effectiveness of the FE modelling.

Strain responses

The strain gage readings in the embedded steel reinforcement predicted by the FE model and measured from experiment are shown in **Fig. 7** and **Fig. 8** for GSCM and GCM, respectively. Apart from the strain gage responses, the responses of the attached LVDTs at the center of the panels were validated. The displacements measured by the LVDTs were converted into strains; these strains are reported in **Fig. 9** along with FE model responses. A good agreement between FE model and test results was observed.

Cracking.

Logarithmic strain plots are shown to represent the crack. The GSCM and the GCM panel failure are shown in **Fig. 10** and **Fig. 11**, respectively; both the FE and the experimental results are shown.

It can be seen that at 1.2 mm of the vertical displacement, in the elastic region of the GSCM panel, logarithmic maximum and minimum principal strains are localised along the diagonal length of the panel. The magnitude of the maximum tensile in-plane strain (horizontal) and the minimum compression in-plane strain (vertical) in the panel are 2330 μ and -1460 μ, respectively. The strain monotonically increases with the increase in the diagonal displacement. The principal tensile and compression strains at failure are 42000μ and -28700μ, respectively. In the GCM panels, the principal tensile strain and compression strain recorded at 1.2 mm diagonal displacement are 2820 μ and -1620 μ, respectively. At failure these strains are 24330 μ and -20730 μ, respectively. These high strains indicate the formation of major cracks.

Furthermore, crushing type failures can be seen in **Fig. 12** near the shoes in the experimental panel. FE model shows such failure through high compressive strain in the exact position as that of experimental test results.

Tensile stress in the reinforcing steel bars

The axial strains measured from the strain gages attached at some selected locations of the reinforcement in the experimental specimens were used to validate the predictions of the steel strains along the length of the reinforcement in the FE model at three stages of loading: 1) elastic, b) peak load and c) failure of the panel. For the elastic region response the diagonal displacement of 1.2 mm was considered. The tensile stress is shown in **Fig. 13**. In the elastic region of the panel, there is no tensile stress on the GSCM panel steel whereas the GCM

panel steel has a very small tensile stress of 2 MPa. At the peak load of their respective panels, the GSCM tensile stress is 38 MPa and the GCM stress is just 5 MPa. Similarly at the ultimate load stage, the GSCM reinforcement has experienced a peak stress of 26 MPa while the GCM exhibited 8 MPa. It can, therefore, be noted that when the peak to ultimate transition occurred, the GSCM panel reinforcement tensile stress reduces while the GCM reinforcement increases. It indicates that the GSCM panel unreinforced masonry is damaged more than that of the GCM panel. From these steel stress levels, it can be concluded that both confining elements remained elastic (no major cracking)-

Comparison with Existing Confined Masonry Models

Some existing confined masonry models are considered in this paper to examine their applicability for the tested specimens. The conversion of the diagonally loaded specimens to the horizontal loading is shown in **Fig. 14**. This conversion assumes that the vertical component of the diagonal load $\left(P \times \sin 45^{\circ}\right)$ is distributed on top of the wall.

The elastic stiffness (K_e) of the diagonally loaded panels is defined in Eq. (4).

$$K_e = E_m \times \frac{A_{su}}{L_{su}} \qquad \text{Eq. (4)}$$

where E_m is the elastic modulus of masonry, and A_{su} and L_{su} are the area and the length of the strut, respectively. The area of the strut (A_{su}) can be estimated from Eq. (5).

$$A_{su} = w_{su} \times t_f \qquad \text{Eq. (5)}$$

where w_{su} is width of the strut and t_f is thickness of face shell area. For the strut width, the definition of Quiroz et al. (2014) was employed. The effective width of the strut is defined as in Eq. (6).

$$w_{su} = (0.35 + 0.022 \times \lambda) \times H \qquad \text{Eq. (6)}$$

where H is height of the wall, and λ is a non-dimensional parameter accounting for the relative stiffness of the confining element, defined as in Eq. (7).

$$\lambda = \frac{E_{ce} \times A_{ce}}{G_m \times A_m} \quad \text{Eq. (7)}$$

where E_{ce} and A_{ce} is elastic modulus and area of the confining element, respectively, and G_m and A_m is shear modulus and area of the unreinforced masonry, respectively. The mean elastic modulus obtained from grouted masonry prism test (14590 MPa) and a grout cylinder test (26000 MPa) was considered for the E_{ce} value of the GSCM and the GCM panels, respectively. The average shear modulus G_m was obtained from the UCM panels as 780 MPa. Using these parameters the non-dimensional relative stiffness parameter (λ) was calculated as 2.5 and 9.6 for the GSCM and the GCM panels, respectively. The effective width of the strut (w_{su}) for the GSCM and the GCM panels was calculated as 344.3 mm and 477.0 mm, respectively. From these results the elastic stiffness of the GSCM panels was calculated as 19.4 kN/mm while the experimental yield stiffness (see **Table 1**) was 16 kN/mm (average of GSCM-A and GSCM-B panels). The GCM panel elastic stiffness was calculated as 26.9 kN/mm and the experimental average stiffness was 27 kN/mm. The formula of strut width (w_{su}) reported in Quiroz et al. (2014)was developed based on the walls constructed similar to the GCM panels construction, therefore its prediction is precise.

The calculated effective width using Eq. (6) was compared with the FE model. For this purpose the vertical stress component of the GSCM and the GCM panels is shown in **Fig. 15**-A and **Fig. 15**-B, respectively. The vertical stress of 1.5 MPa was considered as a minimum strut stress. The measured strut width of GSCM panel at just below its yield load was 330 mm while the equation prediction was 344.3 mm. The FE model strut width for GCM panel at just below its yield load was 485 mm while its equation prediction was 477.0 mm. The FE

352 model exhibits better agreement with the equation prediction for both types of wall. As the
353 strut width of the GSCM panel in the FE model was quite close to the equation prediction, the
354 average stress distribution within the strut was regarded less influential compared to the
355 GCM panel.

356 Further to the panel stiffness analysis, the cracking diagonal load and the ultimate
357 diagonal load of the panels were calculated using existing models and compared with the
358 experimental test results. The details of the models are reported in the appendix. The
359 considered model predictions are shown in **Table 2**. The experimental cracking diagonal load
360 was considered at large inelastic deformation observed at the center of the unreinforced
361 masonry. The cracking diagonal load, the yield diagonal load and the peak diagonal load
362 were calculated using existing confined masonry models and compared with the experimental
363 results. The nomenclature of the equation is denoted as its type of load followed by the three
364 characters that defines the origin of the equation. V_{cr}, V_y and $V_{\max}$ indicate the cracking, the
365 yield and the peak diagonal loads of the panels, respectively. The cracking shear model (
366 V_{cr-Mat}) proposed by Matsumura (1988) was developed from the confined masonry walls
367 constructed similar to the GSCM. Its cracking load prediction is closer to the GSCM panel
368 test results. Matsumura (1988) further developed the model to predict the peak in-plane shear
369 capacity of the partially grouted masonry walls. This model was adopted for the confined
370 masonry wall by AIJ (1999) with a elimination of the horizontal reinforcement terms, which
371 is over-conservative in predicting the peak capacity of the panels. Riahi et al. (2009) equation
372 was developed based on linear regression analysis of 102 confined masonry walls constructed
373 similar to GCM panels. The cracking load predicted by the Riahi et al. (2009) model is
374 closer to the GCM panel results; further the peak diagonal is governed by cracking load
375 hence Riahi et al. (2009) model peak load was 60.3 kN. All peak load expressions include

the masonry and the vertical load terms. Additionally, AIJ (1999) and Riahi et al. (2009) expressions account the contribution from the confining element.

The diagonal yield load of the panels were estimated using the Peruvian national standard SENCICO (2006) expressions. The GSCM panel yield load was predicted by this expression very well within 1.5% variation.

The peak load expressions of the Argentinian (ARG) and Peruvian (PER) equations accounts different level of contribution from the masonry and the vertical load; additionally PER account the wall aspect ratio in its masonry term. PER conservatively predicted the diagonal peak load of the GSCM panel with 4.9% variation and ARG conservatively predicted the diagonal peak load of the GCM panel with 2.2% variation. In general SENCICO (2006) and PER predicted the GSCM loads very well; and ARG predicted the GCM peak load quite well.

Conclusions

In this study, a comparison of direct and indirect confinement of grout to unreinforced masonry behaviors is made. From these comparisons the following conclusions are drawn:

1) The addition of grout into the cores or directly along the edges confines the inscribed unreinforced masonry and increase its diagonal load capacity by 28% and 69%, respectively. The direct confinement is more effective than the indirect confinement through the hollow concrete masonry unit shells. However, the indirect grout confinement is faster to construct (without any need for formwork) and hence may be more cost effective.
2) The masonry initially resists the load by itself while the confinement element does not play a significant role. With the onset of the inelastic behavior (cracking) of the unreinforced masonry, the unreinforced masonry section pushes the confining

elements sideways, which activates the confining element to engage in resisting the loading.

3) The global yield load of the GSCM panel was reached after the unreinforced masonry exhibited its inelastic behavior at 61% of the yield load. However, the GCM panel reached its yield load once unreinforced masonry exhibited inelastic strains at 88% of the yield load.

4) The macro FE model is capable of simulating the behavior of the confined masonry panels with reasonable accuracy. The predictions of the load capacity of the experimental panels, the reinforcement strains, the masonry strains and the crack patters are the predicted appropriately by the FE model.

5) The existing diagonal strut width expression compares well with the predictions of the FE model both for the active and the passive confinements.

6) The confining element itself does not significantly enhance the stiffness of the confined masonry panel; rather stiffer confining elements confine the URM panel well. This aspect increases the effective strut width and hence the stiffness of the confined masonry panel.

7) The following conclusions emerge from the reasonable agreement of the experimental diagonal test results and prediction of the existing confine masonry models:

    a. SENCICO (2006) and Peruvian models predict the GSCM type walls yield and the peak load, respectively.

    b. Argentinian model predicts the GCM type walls peak load capacity well.

It should be recognized that, in spite of the consistent results, the experiments have been carried out from half scale masonry; therefore, further full scale experiments to validate the conclusions would be useful.

Acknowledgements

The authors wish to acknowledge the donation of half scale blocks for the experiment by Mr. David Stubbs, Director of the Canada Masonry Design Center. QUT scholarship and fee waiver to the first author are also thankfully acknowledged.

Notation

A_m = area of the unreinforced masonry;
A_{st} = cross sectional area of the reinforcements in the tie columns;
A_{tc} = tie column cross sectional area;
A_w = net cross sectional area of the confined masonry;
E_c = mean elastic modulus of the concrete (GCM);
E_{ce} = mean elastic modulus of the confining element;
E_{hm} = mean elastic modulus of the hollow masonry;
E_{gm} = mean elastic modulus of the grouted masonry (GSCM);
E_n = elastic modulus normal to the bed joint of the masonry;
E_p = elastic modulus parallel to the bed joint of the masonry;
f_{ce} = compressive strength of confining element;
f_{cn} = uniaxial compressive strength perpendicular to bed joint (masonry);
f_{cp} = uniaxial compressive strength parallel to bed joint (masonry);
f_{hm} = compressive strength of the hollow masonry;
f_{gm} = compressive strength of the grouted masonry;
$f_m^{'}$ = characteristic compressive strength of the masonry;
$f_{m,(g)}^{'}$ = characteristic compressive strength of the masonry in gross area terms;
f_{mt} = mean flexural tensile strength of the masonry;
f_{tn} = uniaxial tensile strength perpendicular to bed joint (masonry);
f_{tp} = uniaxial tensile strength parallel to bed joint (masonry);
f_{yvc} = yield strength of the reinforcements located in the tie columns;
G_m = shear modulus of the masonry;
G_{tn} = energy for tension failure normal to the bed joint;
G_{tp} = energy for tension failure parallel to the bed joint;
H = wall height;
h = height of the unreinforced masonry in the confined masonry;
$\overline{h}$ = characteristic length of the element;
$j = \frac{7}{8} L_e$;

L = length of the wall.

L_e = effective length of the wall (Extreme compression fiber to tension bar);

L_{su} = length of the diagonal strut;

K_e = elastic stiffness of the panel;

K_u = ultimate stiffness of the panel;

K_y = yield stiffness of the panel;

$k_p = 1.16 p_t^{0.3}$ - 1 for fully grouted masonry; and 0.6 for partially grouted concrete masonry;

k_u = 1 for fully grouted masonry; and 0.6 for partially grouted concrete masonry;

P = diagonal tension load;

$p_t = \frac{A_{st}}{t \times L_e}$;

t = thickness of the wall;

t_f = facially bedded thickness of the wall;

V_{cr} = in-plane horizontal cracking load;

V_y = in-plane horizontal yield load;

$V_{\max}$ = in-plane horizontal peak load;

v_m = shear strength of the masonry from diagonal tension test;

w_{su} = width of the diagonal strut;

S_p = stiffness degradation at the peak load;

S_u = stiffness degradation at the ultimate load;

κ_c = scalar controls the amount of hardening and softening in compression;

κ_t = scalar controls the amount of softening in tension;

σ_n = stress perpendicular/ normal to bed joints;

σ_p = stress parallel to bed joints;

σ_v = vertical stress applied on the wall;

$\sigma_{v,(g)}$ = vertical stress applied on the wall in gross area terms;

τ_{np} = shear stress in n-p plane;

τ_u = pure shear strength;

α = shear stress contribution factor to the tension failure;

β = biaxial compression strength factor;

γ = shear stress contribution factor to the compression failure;

α_{ce} = 1.0 for fully grouted masonry and 0.6 for partially grouted masonry;

β_{ce} = reduction factor for shear due to the slenderness ratio;

$\gamma_{ce} = \frac{H}{L}, \frac{1}{3} \le \gamma_{ce} \le 1$;

$\rho_{vc} = \frac{A_{st}}{A_{tc}}$;

References

1. AIJ (Architectural Institute of Japan). (1999). "Ultimate strength and deformation capacity of buildings in seismic design, committee for concrete and masonry wall building structures." Tokyo, 592-593.
2. AS (Australian standards). (2009). "Australian standard of concrete structures ." *AS 3600*, Australia, Standards Australia Limited.
3. AS (Australian standards). (2011). "Australian standard of masonry structures." *AS 3700*, Standards Australia Limited.
4. AS/NZS (Australian and New Zealand standards). (2003a). "Masonry units. Segmental pavers and flags- methods of test. Method 4: Determining compressive strength of masonry units." *AS/NZS 4456.4*, Australia, Standards Australia Limited and Standards New Zealand.
5. AS/NZS (Australian and New Zealand standards). (2003b). "Australian/new zealand standrd of masonry units, segmental pavers and flags method of test. Determining lateral modulus of rupture." *AS/NZS 4456.15*, Standards Australia Limited and Standards New Zealand.
6. ASTM (American Society for Testing and Materials). (2009). "Standard test methods and definitions for mechanical testing of steel products." *ASTM A370*, U.S.A, ASTM International.
7. ASTM (American Society for Testing and Materials). (2006). "Standard test method for sieve analysis of fine and coarse aggregates." *ASTM C136-06*, U.S.A, ASTM International.
8. ASTM (American Society for Testing and Materials). (2002). "Standard test method for diagonal tension (shear) in masonry assemblages." *ASTM E519-02*, U.S.A, ASTM International.
9. Corradi, M., Tedeschi, C., Binda, L., and Borri, A. (2008). "Experimental evaluation of shear and compression strength of masonry wall before and after reinforcement: Deep repointing." *Construction and Building Materials. 22*(4), 463-472.
10. Dhanasekar, M., and Haider, W. (2008a, 2008). "On the inplane shear and simplified design provisions for reinforced masonry in as3700." *Proc., Australian Structural Engineering Conference.* Melbourne, Australia, 133-145.
11. Dhanasekar, M., and Haider, W. (2008b). "Explicit finite element analysis of lightly reinforced masonry shear walls." *Computers & Structures. 86*(1-2), 15-26.
12. Dizhur, D., Griffith, M., and Ingham, J. (2013). "In-plane shear improvement of unreinforced masonry wall panels using nsm cfrp strips." *Journal of Composites for Construction.* 10.1061/(ASCE)CC.1943-5614.0000400, 04013010.
13. Haider, W. (2007). "In-plane response of wide spaced reinforced masonry shear walls." (*PhD thesis*), Central Queensland University. , Australia
14. Janaraj, T. (2014). "Studies on the in-plane shear response of confined masonry shear walls." (*PhD thesis*), Queensland University of Technology, Australia, Australia.
15. Janaraj, T., and Dhanasekar, M. (2014). "Finite element analysis of the in-plane shear behaviour of masonry panels confined with reinforced grouted cores." *Construction and Building Materials. 65*(0), 495-506.
16. Lourenço, P. B. (1996). "*Computational strategies for masonry structures."* Delft university press, Delft University, Netherlands
17. Matsumura, A. (1988). "Shear strength of reinforced masonry walls." *Proc., 9th World Conf. on Earthquake Engineering.* Tokyo, 121-126.

18. Medeiros, P., Vasconcelos, G., Lourenço, P. B., and Gouveia, J. (2013). "Numerical modelling of non-confined and confined masonry walls." *Construction and Building Materials. 41*(0), 968-976.
19. Moroni, M., Astroza, M., and Acevedo, C. (2004). "Performance and seismic vulnerability of masonry housing types used in chile." *Journal of Performance of Constructed Facilities.* 10.1061/(ASCE)0887-3828(2004)18:3(173).
20. Nolph, S. M., and ElGawady, M. A. (2012). "Static cyclic response of partially grouted masonry shear walls." *Journal of Structural Engineering.* 10.1061/(ASCE)ST.1943-541X.0000529, 864-879.
21. Quiroz, L. G., Maruyama, Y., and Zavala, C. (2014). "Cyclic behavior of peruvian confined masonry walls and calibration of numerical model using genetic algorithms." *Engineering Structures. 75*(0), 561-576.
22. Riahi, Z., Elwood, K., and Alcocer, S. (2009). "Backbone model for confined masonry walls for performance-based seismic design." *Journal of Structural Engineering.* doi:10.1061/(ASCE)ST.1943-541X.0000012, 644-654.
23. SENCICO (National Training Service for the Construction Industry). (2006). "Technical standard for masonry." *E.070*, Lima, Peru, National Building Regulations.
24. Shing, P. B., Schuller, M., and Hoskere, V. S. (1990). "In-plane resistance of reinforced masonry shear walls." *Journal of Structural Engineering.* 10.1061/(ASCE)0733-9445(1990)116:3(619).
25. Tena-Colunga, A., Juárez-Ángeles, A., and Salinas-Vallejo, V. H. (2009). "Cyclic behavior of combined and confined masonry walls." *Engineering Structures. 31*(1), 240-259. 10.1016/j.engstruct.2008.08.015.
26. Van der Pluijm, R. (1997). "Non-linear behaviour of masonry under tension." *Heron-English edition. 42*, 25-54.
27. Yoshimura, K., Kikuchi, K., Okamoto, T., and Sanchez, T. (1996). "Effect of vertical and horizontal wall reinforcement on seismic behavior of confined masonry walls." *Proc., Eleventh World Conference on EarthquakeEnigineering.* Mexico, 191-198.

Appendix: Some Selected Reinforced Masonry Shear Capacity Equations

Matsumura (1988) cracking model is shown in Eq. (8). V_{cr-Mat} measures the cracking strength.

$$V_{cr-Mat} = \left\{ \frac{\mathrm{k}_u}{\left(h / L_e\right) + 2} \sqrt{f'_{m,(g)}} + 0.3 \times \alpha_{ce} \times \sigma_{v,(g)} \right\} \mathrm{t} \times \mathrm{j} \qquad \text{Eq. (8)}$$

The cracking strength model proposed by Riahi et al. (2009) is shown in Eq. (9).

$$V_{cr-Ria} = (0.424 v_m + 0.374 \sigma_v)\, \mathrm{A}_w \le v_m\, \mathrm{A}_w \qquad \text{Eq. (9)}$$

The yield strength prediction model published in SENCICO (2006) is shwon in Eq. (10).

$$V_{y-Sen} = 0.5(\beta_{ce})(v'_m) A_w + 0.23 \sigma_v \times A_w \qquad \text{Eq. (10)}$$

The peak shear strength predicting model published in AIJ (1999) is shown in Eq. (11), where $V_{\max-AIJ}$ indicates peak shear strength of the model.

$$V_{\max-AIJ} = \left[k_u k_p \left(\frac{0.76}{h/L_e + 0.7} + 0.012 \right) \sqrt{f'_{m,(g)}} + 0.2 \times \sigma_{v,(g)} \right] \text{t} \times \text{j} \qquad \text{Eq. (11)}$$

The peak shear strength model proposed by the Riahi et al. (2009) is shown in Eq. (12), where $V_{\max-\text{Ria}}$ indicates peak shear strength of the model.

$$V_{\max-\text{Ria}} = \left(0.21 \text{v}_m + 0.363\sigma_v + 0.0141\sqrt{\rho_{vc} f_{yvc} f_{ce}} \right) A_w \geq V_{cr-Ria} \qquad \text{Eq. (12)}$$

Another two peak strength predicting models obtained from Riahi et al. (2009) is shown in Eq. (13) and Eq. (14), respectively. Where $V_{\max-PER}$ and $V_{\max-ARG}$ were originally pubilished in Peruvian standards and Argentinian standards, respectively.

$$V_{\max-PER} = (0.5 \times \gamma_{ce} \times v_m + 0.23\sigma_v) \text{A}_w \qquad \text{Eq. (13)}$$

$$V_{\max-ARG} = (0.6v_m + 0.3\sigma_v) \text{A}_w \qquad \text{Eq. (14)}$$

List of Figures.

List of Tables.

Table 1. Test results of the specimens

Specimen Name	Diagonal peak load in kN/ drift in %.	k_y (kN/mm)	k_P (kN/mm)	k_u (kN/mm)	S_p (%)	S_u (%)
UCM-A	45.6/ 0.33	15.9	14.9	9.8	-6.3	-38.4
UCM-B	51.6/ 0.37	16.1	14.9	9.5	-7.5	-41
GSCM-A	58.4/ 0.36	15.5	13.4	9.0	-13.5	-41.9
GSCM-B	63.1/ 0.36	16.5	14.7	9.4	-10.9	-43
GCM-A	80.3/ 0.29	27	22.7	10.2	-15.9	-62.2
GCM-B	75.8/ 0.27	26.9	23.1	12.7	-14.1	-52.8

618 **Table 2**. Prediction of existing confined masonry models

Equations (references)	Predicted diagonal load in kN		Experimental Peak Load kN	
	GSCM	GCM	GSCM average (A & B)	GCM average (A & B)
V_{cr-Mat} (refer Eq. (8)) (Matsumura 1988)	42.9	42.9	35 (33 & 36)	68 (75 & 61)
V_{cr-Ria} (refer Eq. (9)) (Riahi et al. 2009)	60.3	60.3		
V_{y-Sen} (refer Eq. (10)) (SENCICO 2006)	57.8	57.8	58.7 (56.3 & 61.1)	69.2 (76.9 & 61.4)
$V_{max-AIJ}$ (refer Eq. (11)) (AIJ 1999)	44.0	44.0		
$V_{max-Ria}$ (refer Eq. (12)) (Riahi et al. 2009)	60.3	60.3	60.8 (58.4 & 63.1)	78.1 (80.3 & 75.8)
$V_{max-PER}$ (refer Eq. (13)) (Peruvian equation taken from Riahi et al. (2009))	57.8	57.8		
$V_{max-ARG}$ (refer Eq. (14)) (Argentinian equation taken from Riahi et al. (2009))	76.4	76.4		

619

Table 1. Test results of the specimens

Specimen Name	Diagonal peak load in kN/ drift in %.	k_y (kN/mm)	k_P (kN/mm)	k_u (kN/mm)	S_p (%)	S_u (%)
UCM-A	45.6/ 0.33	15.9	14.9	9.8	-6.3	-38.4
UCM-B	51.6/ 0.37	16.1	14.9	9.5	-7.5	-41
GSCM-A	58.4/ 0.36	15.5	13.4	9.0	-13.5	-41.9
GSCM-B	63.1/ 0.36	16.5	14.7	9.4	-10.9	-43

Table 2. Prediction of existing confined masonry models

Equations (references)	Predicted diagonal load in kN		Experimental results in kN	
	GSCM	GCM	GSCM average (A & B)	GCM average (A & B)
$V_{cr-Mat} = \left\{ \frac{k_u}{(h/L_e)+2} \sqrt{f'_{m,(g)}} + 0.3 \times \alpha_{ce} \times \sigma_{v,(g)} \right\} t \times j$ (Matsumura 1988)	42.9	42.9	35 (33 & 36)	68 (75 & 61)
$V_{cr-Ria} = (0.424 v_m + 0.374 \sigma_v) A_w \le v_m A_w$ (Riahi et al. 2009)	60.3	60.3		
$V_{y-Sen} = 0.5(\beta_{ce})(v'_m) A_w + 0.23 \sigma_V \times A_w$ (SENCICO 2006)	57.8	57.8	58.7 (56.3 & 61.1)	69.2 (76.9 & 61.4)
$V_{max-AIJ} = \left[k_u k_p \left(\frac{0.76}{h/L_e + 0.7} + 0.012 \right) \sqrt{f'_{m,(g)}} + 0.2 \times \sigma_{v,(g)} \right] t \times j$ (AIJ 1999)	44.0	44.0		
$V_{max-Ria} = \left(0.21 v_m + 0.363 \sigma_v + 0.0141 \sqrt{\rho_{vc} f_{yvc} f_{ce}} \right) A_w \ge V_{cr-Ria}$ (Riahi et al. 2009)	60.3	60.3	60.8 (58.4 & 63.1)	78.1 (80.3 & 75.8)
$V_{max-PER} = (0.5 \times \gamma_{ce} \times v_m + 0.23 \sigma_v) A_w$ (Peruvian equation taken from Riahi et al. (2009))	57.8	57.8		
$V_{max-ARG} = (0.6 v_m + 0.3 \sigma_v) A_w$ (Argentinian equation taken from Riahi et al. (2009))	76.4	76.4		

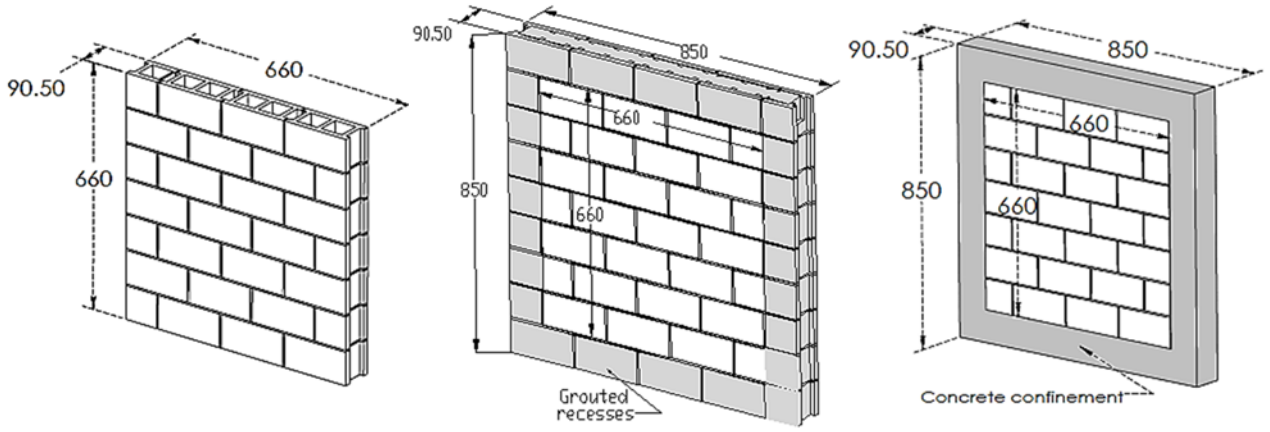

A) Unconfined Masonry (UCM)

B) Core Filled confined masonry panel(GSCM)

C) Formwork Based confined masonry panel(GCM)

Fig. 1. Unconfined and Confined Panels

A) GSCM panel construction

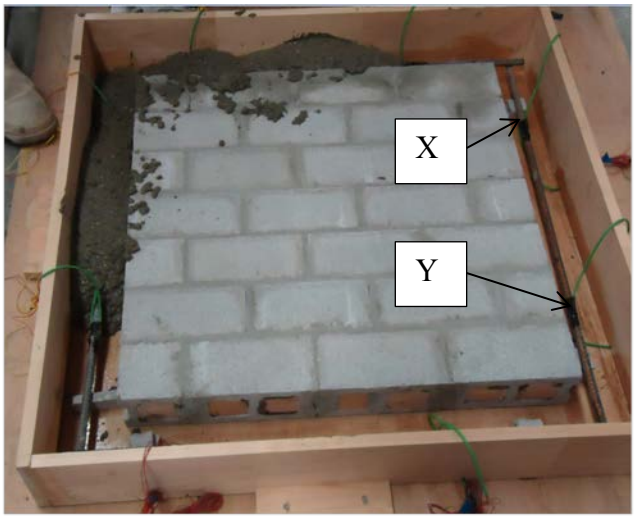

B) GCM panel construction

Fig. 2. Confined masonry panel constructions

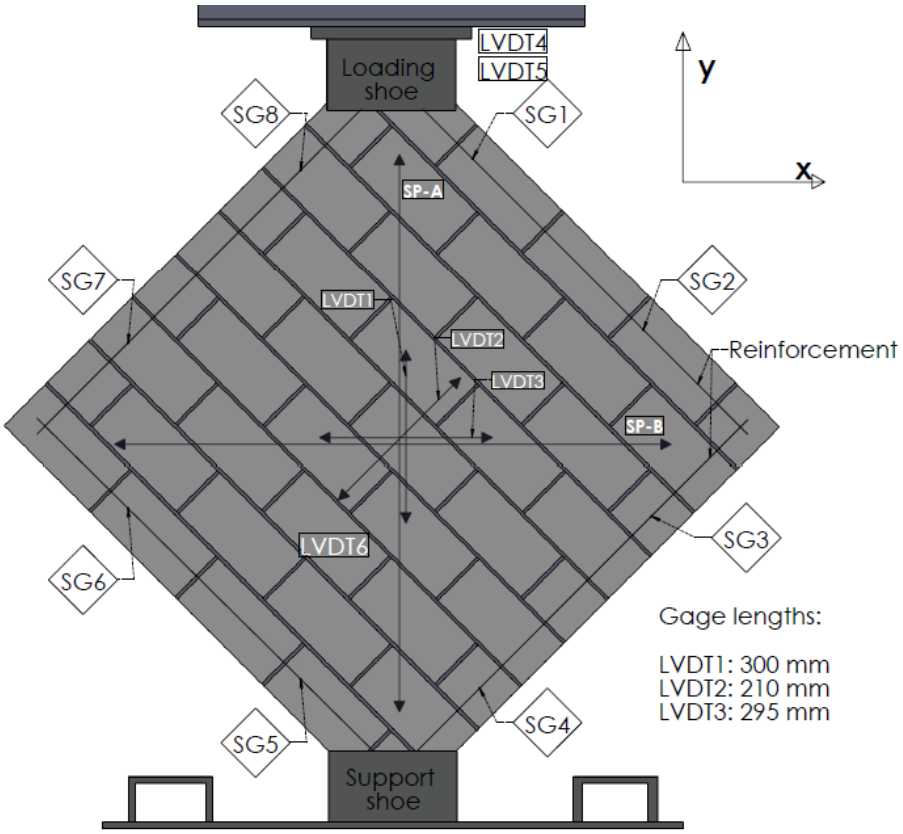

Fig. 3. Schematic scheme of instrumentation of GSCM/ GCM panels

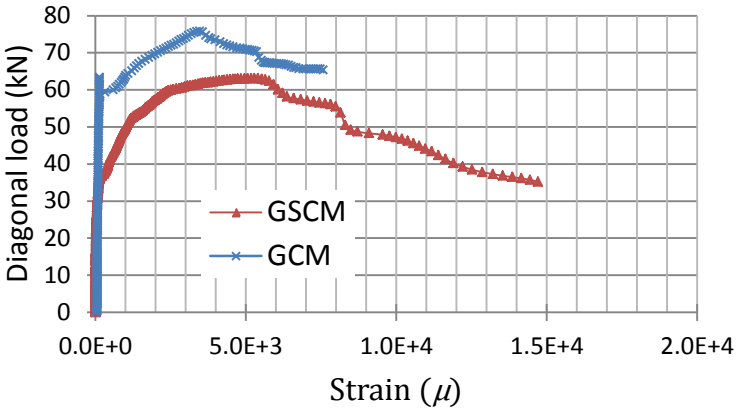

(A)- Maximum principal strain (tension)

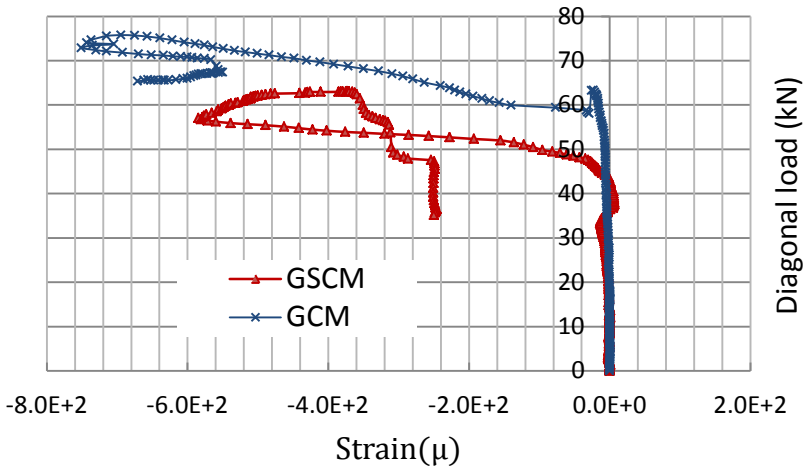

(B)- Minimum principal strain (compression)

Fig. 4. Diagonal load versus URM principal strains.

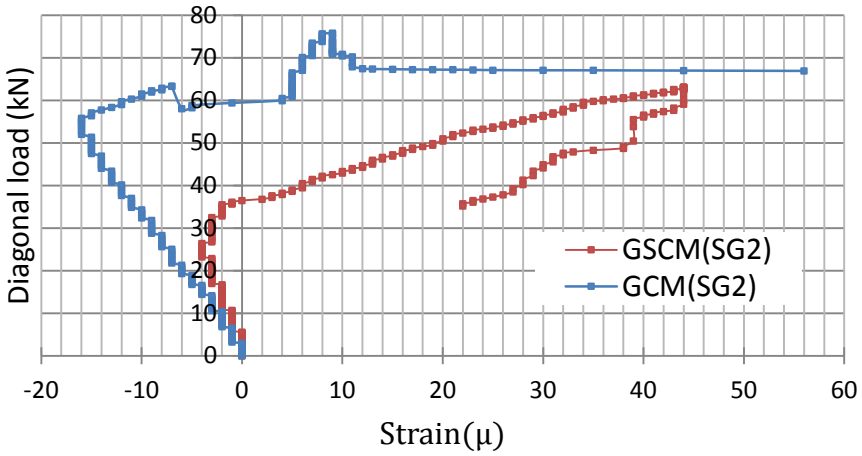

Fig. 5. Principal strain in the reinforcement (SG2)

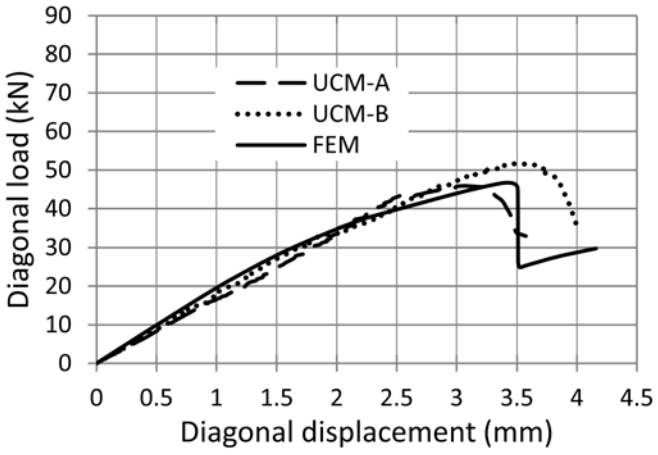

A) UCM

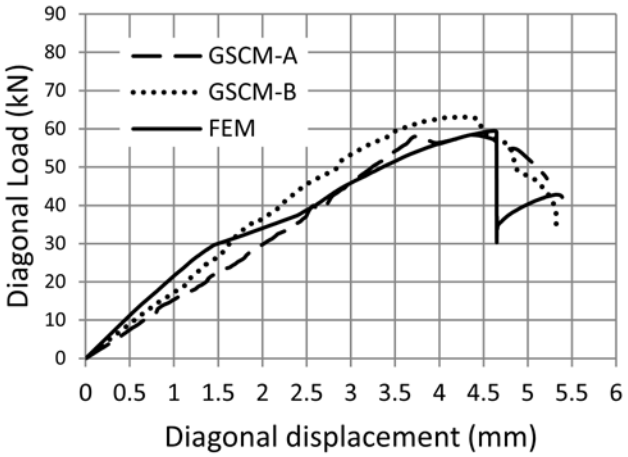

B) GSCM

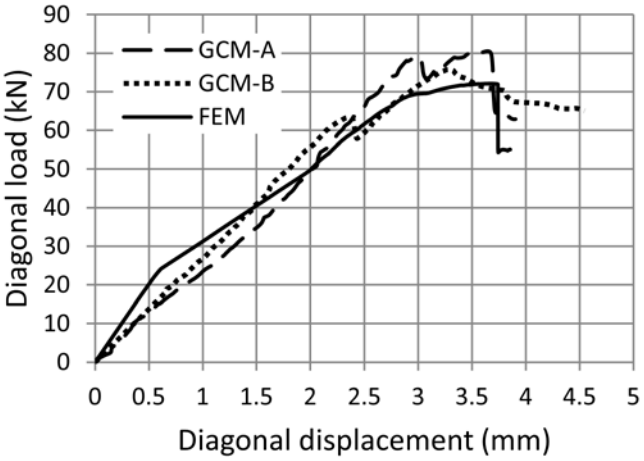

C) GCM

Fig. 6. Load versus displacement

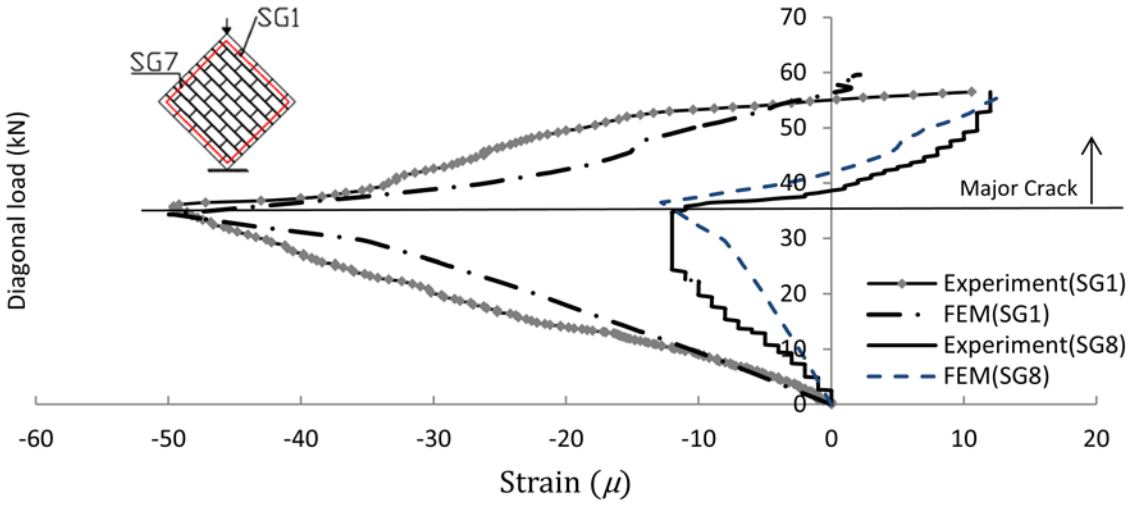

Fig. 7. Diagonal load versus reinforcing bar strain for GSCM panel

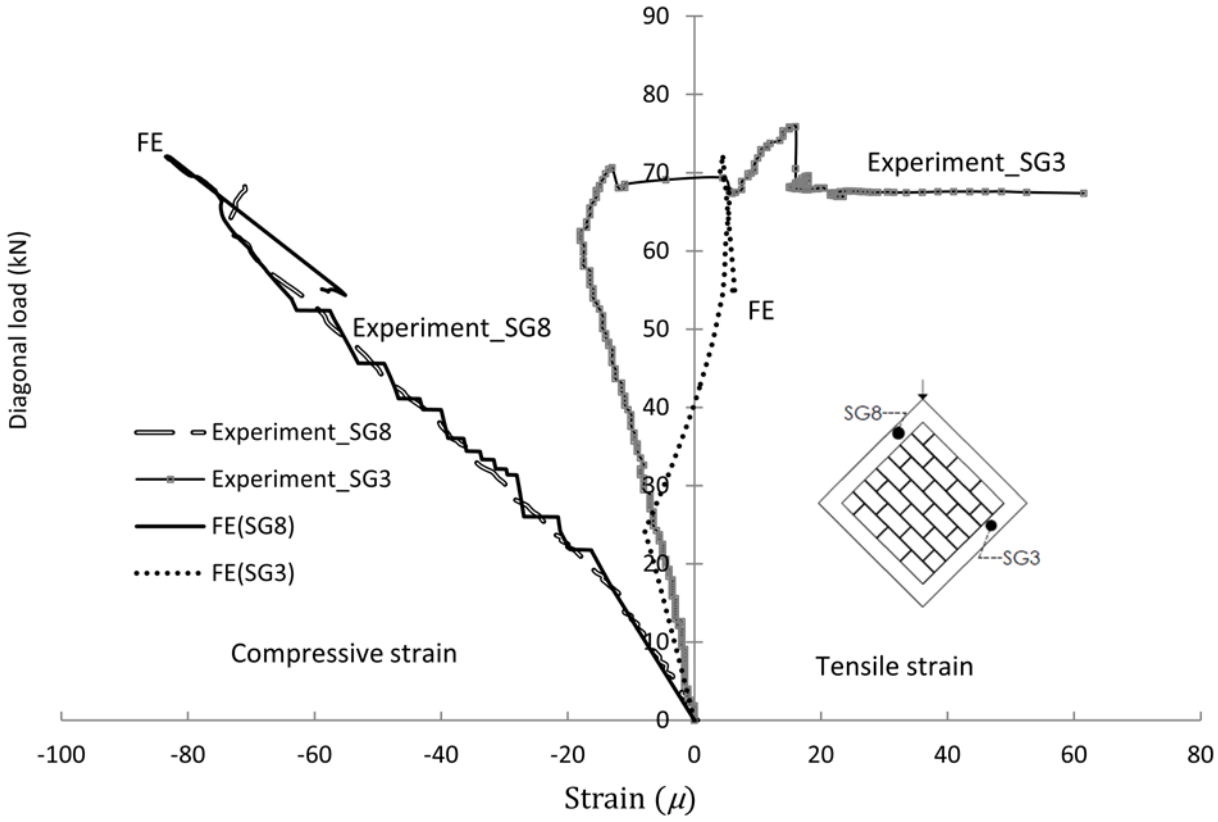

Fig. 8. Strain on the embedded reinforcing bar in GCM panel.

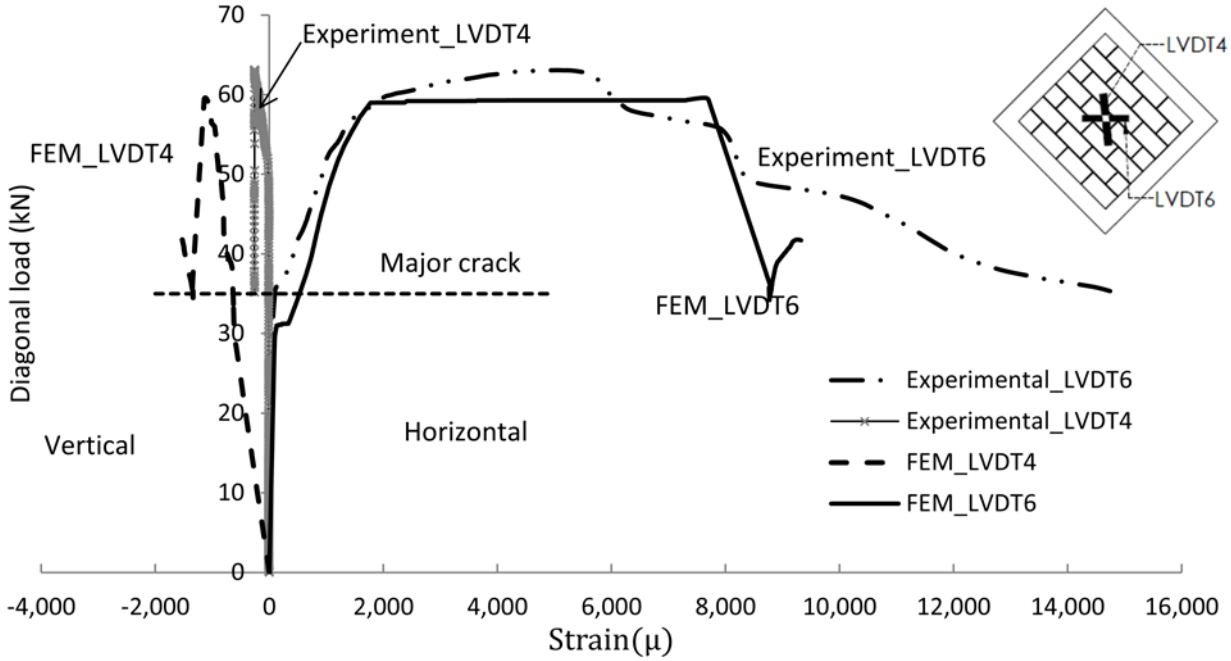

Fig. 9. Diagonal load versus strain at center

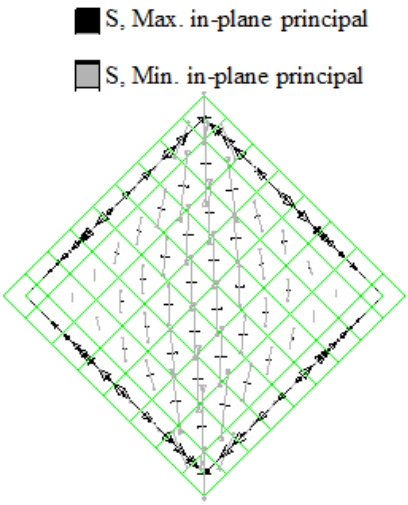

A) Principal stresses at displacement of 1.2 mm (elastic).

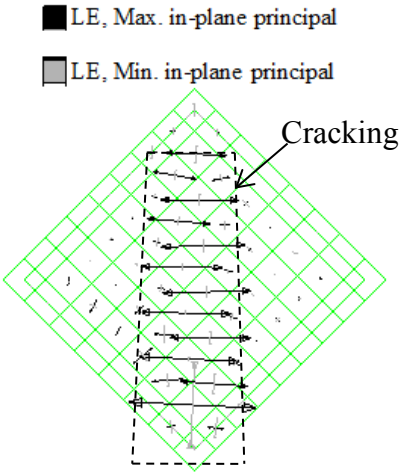

B) Principal strains at displacement of 5.1 mm (failure).

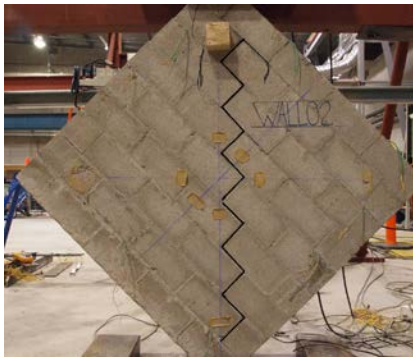

C) Experimental panel at failure.

Fig. 10. Failure of GSCM panel

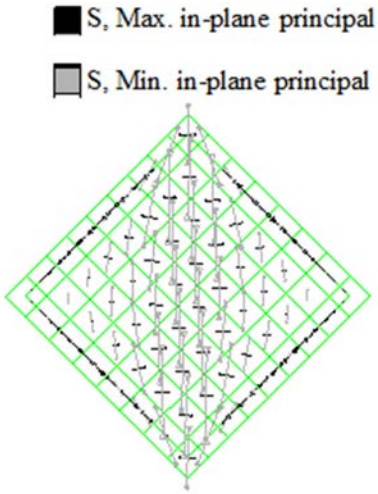

A) Principal stresses at displacement of 1.2 mm (elastic).

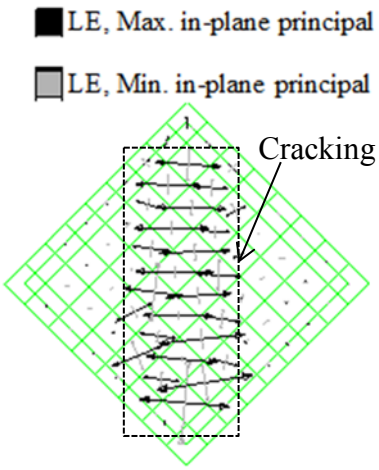

B) Principal strains at displacement of 3.85 mm (failure).

C) Experimental panel at failure.

Fig. 11. Failure of GCM panel

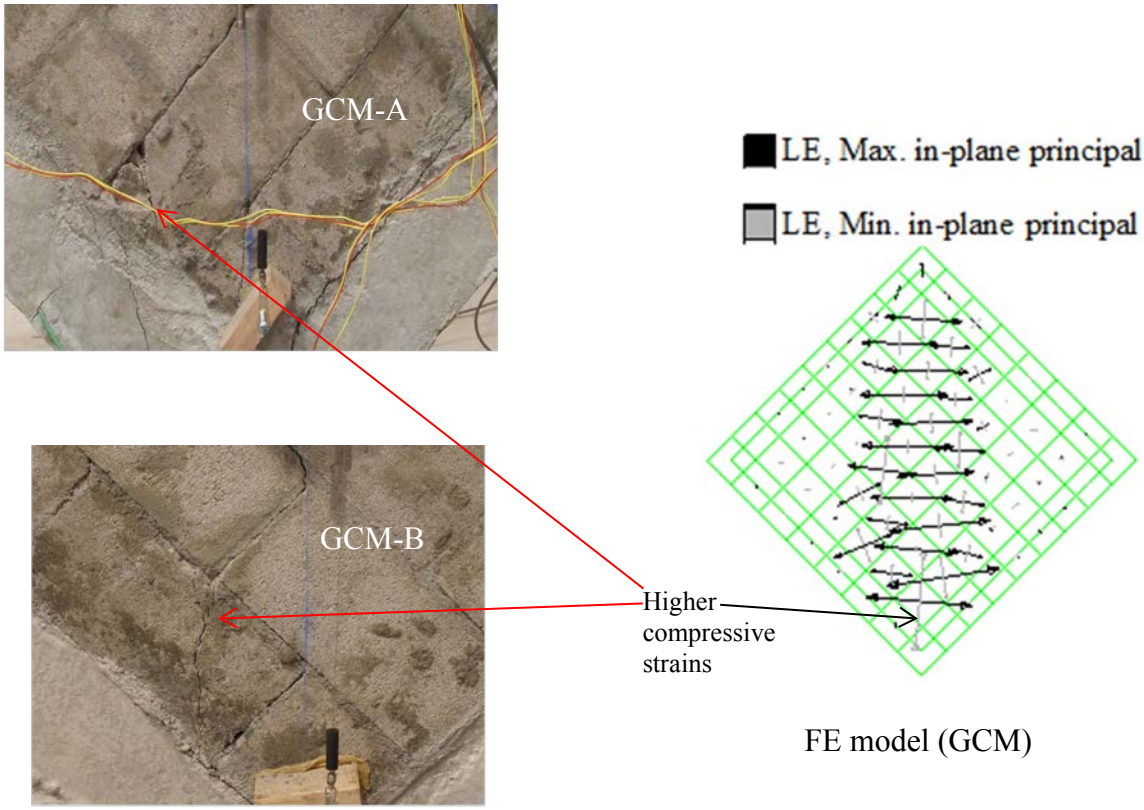

Fig. 12. Block crushing and FE prediction

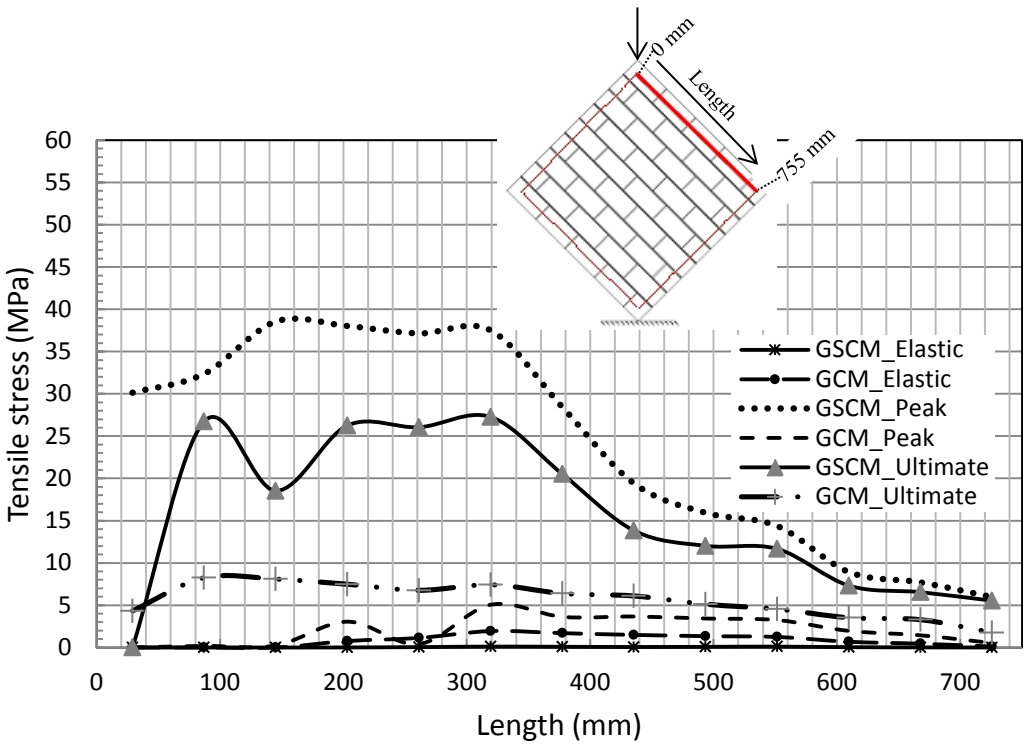

Fig. 13. Tensile stresses on the steel

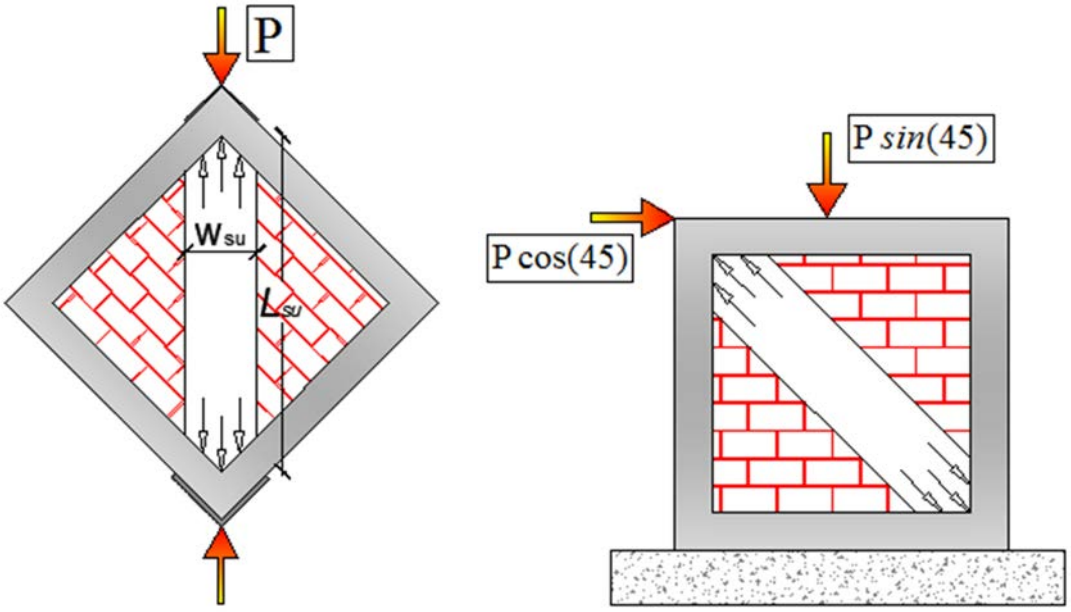

a) Diagonal loading b) Equivalent horizontal loading

Fig. 14. Diagonal loading versus horizontal loading